PHYSICAL REVIEW D **71,** 044009 (2005)

General relativistic model for the gravitational field of active galactic nuclei surrounded by a disk

D. Vogt*
Instituto de Física Gleb Wataghin, Universidade Estadual de Campinas, 13083-970 Campinas, S. P., Brazil

P. S. Letelier†
Departamento de Matemática Aplicada-IMECC, Universidade Estadual de Campinas, 13083-970 Campinas, S. P., Brazil
(Received 26 August 2004; published 9 February 2005)

An exact but simple general relativistic model for the gravitational field of active galactic nuclei is constructed, based on the superposition in Weyl coordinates of a black hole, a Chazy-Curzon disk and two rods, which represent matter jets. The influence of the rods on the matter properties of the disk and on its stability is examined. We find that in general they contribute to destabilize the disk. Also the oscillation frequencies for perturbed circular geodesics on the disk are computed, and some geodesic orbits for the superposed metric are numerically calculated.

DOI: 10.1103/PhysRevD.71.044009 PACS numbers: 04.40.–b, 04.20.Jb, 98.58.Fd, 98.62.Mw

I. INTRODUCTION

There is strong observational evidence that active galactic nuclei (AGN), X-ray transients and gamma-ray bursts (GRBs) are associated with accretion onto black holes, and that these sources are able to form collimated, ultrarelativistic flows (relativistic jets).

The exact mechanisms to explain the production of jets are still uncertain, but they probably involve the interaction between a spinning black hole, the accretion disk, and electromagnetic fields in strong gravitational fields (see, for example, [1–3] and references therein).

Thus, a reasonably accurate general relativistic model of an AGN would require an exact solution of Einstein-Maxwell field equations that describes a superposition of a Kerr black hole with a stationary disk and electromagnetic fields. Not even an exact solution of a stationary black hole-disk system has been found yet. Solutions for static thin disks without radial pressure were first studied by Bonnor and Sackfield [4], and Morgan and Morgan [5], and with radial pressure by Morgan and Morgan [6]. Several classes of exact solutions of the Einstein field equations corresponding to static thin disks with or without radial pressure have been obtained by different authors [7–16]. Thin rotating disks were considered in [17,18]. Perfect fluid disks with halos [19] and charged perfect fluid disks [20] were also studied, whereas thick relativistic disks were reported in [21]. Several solutions of the Einstein equations coupled to matter that represent disks have also been studied by the Jena group [22–29].

The static superposition of a disk and a black hole was first considered by Lemos and Letelier [10]. Zellerin and Semerák [30] found a stationary metric that reduces to the superposition of a disk and a black hole in the static limit and thus may represent a stationary disk-black hole system. The analysis of their solution is complicated by the fact that the metric functions cannot be analytically computed. For a survey on self-gravitating relativistic thin disks, see for instance [31].

The aim of this paper is to consider the gravitational field of an AGN through a simple model: the *static* superposition of a black hole with a Chazy-Curzon disk and two rods placed on the symmetry axis, which will represent jets. Our principal interest here is to see how the presence of the rods affect the matter properties and stability of the disk.

The article is divided as follows. In Sec. II we review the "displace, cut and reflect" method used to construct thin disks from a known solution of Einstein field equations in Weyl coordinates. Section III summarizes the formalism to superpose thin disks and other Weyl solutions. Section IV discusses Schwarzschild solution and the metric of a finite rod in Weyl coordinates. In Sec. V the results of Secs. III and IV are then applied to construct the superposition of disk, black hole and rods and the resulting energy-momentum tensor. In Sec. VI the disk stability is studied through small horizontal and vertical oscillations about equatorial circular geodesics. In Sec. VII some geodesic orbits for the superposed metric are numerically calculated. Finally, Sec. VIII is devoted to discussion of the results. We take units such that $c = G = 1$.

II. THIN DISK SOLUTIONS IN WEYL COORDINATES

In absence of matter, the general metric for a static axially symmetric spacetime in Weyl's canonical coordinates (t, r, z, φ) is given by

$$ds^2 = -e^{\phi}dt^2 + e^{\nu-\phi}(dr^2 + dz^2) + r^2e^{-\phi}d\varphi^2, \quad (1)$$

where ϕ and ν are functions of r and z only. Einstein vacuum field equations for the metric Eq. (1) yield [32,33]

*Electronic address: danielvt@ifi.unicamp.br
†Electronic address: letelier@ime.unicamp.br

$$\phi_{,rr} + \frac{\phi_{,r}}{r} + \phi_{,zz} = 0, \tag{2a}$$

$$\nu[\phi] = \frac{1}{2}\int r[(\phi_{,r}^2 - \phi_{,z}^2)\mathrm{d}r + 2\phi_{,r}\phi_{,z}\mathrm{d}z]. \tag{2b}$$

Given a solution of Eqs. (2a) and (2b), one can construct a thin disk by using the well known "displace, cut and reflect" method, due to Kuzmin [34]. First, a surface ($z = 0$) is chosen so that it divides the usual space in two parts: one with no singularities or sources, and the other with them. Then the part of the space with singularities or sources is disregarded. At last, the surface is used to make an inversion of the nonsingular part of the space. The result will be a space with a singularity that is a delta function with support on $z = 0$. The method is mathematically equivalent to making a transformation $z \to |z| + a$, where a is a constant.

The application of the formalism of distributions in curved spacetimes to the Weyl metric Eq. (1) is exposed in [13]. One finds that the components of the distributional energy-momentum tensor $[T^a_b]$ on the disk are

$$-T^t{}_t = e^{\phi-\nu}(2 - r\phi_{,r})\phi_{,z}\delta(z), \tag{3}$$

$$T^\varphi{}_\varphi = e^{\phi-\nu}r\phi_{,r}\phi_{,z}\delta(z), \tag{4}$$

$$T^r{}_r = T^z_z = 0, \tag{5}$$

where $\delta(z)$ is the Dirac distribution with support on the disk and is understood that $\phi_{,z} = \lim_{z\to 0^+}\phi_{,z}$. The "true" energy density and azimuthal pressure are, respectively,

$$\sigma = e^{(\nu-\phi)/2}(-T^t_t), \tag{6}$$

$$p = e^{(\nu-\phi)/2}T^\varphi_\varphi. \tag{7}$$

To explain the disk stability in absence of radial pressure, one may assume the counter-rotating hypothesis, where the particles on the disk move in such a way that there are as many particles moving in clockwise as in counterclockwise direction. The velocity V of counter-rotation of the particles in the disk is given by [9,35]

$$V^2 = \frac{p}{\sigma} \tag{8}$$

If $V^2 < 1$, the particles travel at sublumial velocities. The specific angular momentum h of particles on the disk moving in circular orbits along geodesics reads

$$h = r^{3/2}e^{-\phi/2}\sqrt{\frac{\phi_{,r}}{2(1 - r\phi_{,r})}}. \tag{9}$$

The stability of circular orbits on the disk plane can be determined with an extension of Rayleigh criteria of stability of a fluid at rest in a gravitational field: $h\frac{\mathrm{d}h}{\mathrm{d}r} > 0$ [36]. Using Eq. (9) this is equivalent to

$$\phi_{,r}(-3r\phi_{,r} + 3 + r^2\phi_{,r}^2) + r\phi_{,rr} > 0. \tag{10}$$

III. SUPERPOSITION OF THIN DISKS AND OTHER WEYL SOLUTIONS

An important property of the Weyl metric Eq. (1) is that the field Eq. (2a) for the potential ϕ is the Laplace equation in cylindrical coordinates. Since Laplace's equation is linear, if ϕ_1 and ϕ_2 are solutions, then the superposition $\phi = \phi_1 + \phi_2$ is also a solution. The other metric function Eq. (2b) is nonlinear, and so cannot be superposed. But one can show that the relation

$$\nu[\phi_1 + \phi_2] = \nu[\phi_1] + \nu[\phi_2] + 2\nu[\phi_1, \phi_2], \tag{11}$$

where

$$\nu[\phi_1, \phi_2] = \frac{1}{2}\int r[(\phi_{1,r}\phi_{2,r} - \phi_{1,z}\phi_{2,z})\mathrm{d}r + (\phi_{1,r}\phi_{2,z} + \phi_{1,z}\phi_{2,r})\mathrm{d}z], \tag{12}$$

holds. Other useful relations are given in [8].

The energy-momentum tensor of the combined system disk and black hole has been computed by Lemos and Letelier [13]. Let ϕ_D and ϕ_{BH} be the metric potentials of the disk and of the black hole, respectively. Then the components $[T^a_b]$ of the superposition are

$$-T^t{}_t = e^{\phi_D+\phi_{BH}-\nu}[2 - r(\phi_D + \phi_{BH})_{,r}]\phi_{D,z}\delta(z), \tag{13}$$

$$T^\varphi{}_\varphi = e^{\phi_D+\phi_{BH}-\nu}r(\phi_D + \phi_{BH})_{,r}\phi_{D,z}\delta(z), \tag{14}$$

$$T^r{}_r = T^z_z = 0, \tag{15}$$

where $\nu = \nu[\phi_D + \nu_{BH}]$, and again $\phi_{D,z} = \lim_{z\to 0^+}\phi_{D,z}$. The true energy density and azimuthal pressure read

$$\sigma = e^{(\nu-\phi_D-\phi_{BH})/2}(-T^t{}_t), \tag{16}$$

$$p = e^{(\nu-\phi_D-\phi_{BH})/2}T^\varphi{}_\varphi. \tag{17}$$

Equation (13) and (14) show that the potential of the black hole interacts with the disk and changes its matter properties. Although Eqs. (13)–(17) have been derived for superposition of disk and black hole, they are also valid when the potential function ϕ_{BH} is a sum of other Weyl solutions, like the superposition of a black hole and rods.

IV. BLACK HOLES AND RODS IN WEYL COORDINATES

The Schwarzschild black hole metric function ϕ_{BH} in Weyl coordinates is given by

$$\phi_{BH} = \ln\left(\frac{r_1 + r_2 - 2M}{r_1 + r_2 + 2M}\right), \tag{18}$$

where $r_1^2 = (M - z)^2 + r^2$ and $r_2^2 = (M + z)^2 + r^2$. The function $\phi(r, z)$ can be related to the Newtonian potential U by

$$\phi = 2U. \tag{19}$$

Thus, the metric potential ϕ_R of a finite rod of linear mass density λ lying on the z axis and located along $[c_1, c_2]$ is

$$\phi_R = -2\lambda \ln\left[\frac{c_2 - z + \sqrt{r^2 + (c_2 - z)^2}}{c_1 - z + \sqrt{r^2 + (c_1 - z)^2}}\right]. \quad (20)$$

The calculation of the other metric function ν for Eqs. (18) and (20) and later for the superposed metric, is considerably simplified when one defines the following μ function

$$\mu_k = \alpha_k - z + \sqrt{r^2 + (\alpha_k - z)^2}, \quad (21)$$

where α_k is an arbitrary constant. This function is a natural consequence of the formalism of the inverse scattering method [37,38]. Equations (18) and (20) can be rewritten as

$$\phi_{BH} = \ln\left(\frac{\mu_1}{\mu_2}\right), \quad (22)$$

$$\phi_R = -2\lambda \ln\left(\frac{\mu_3}{\mu_4}\right), \quad (23)$$

where we defined

$$\mu_1 = -M - z + \sqrt{r^2 + (M + z)^2},$$
$$\mu_2 = M - z + \sqrt{r^2 + (M - z)^2},$$
$$\mu_3 = c_2 - z + \sqrt{r^2 + (c_2 - z)^2},$$
$$\mu_4 = c_1 - z + \sqrt{r^2 + (c_1 - z)^2}.$$

On using Eq. (11)

$$\nu[\ln\mu_i - \ln\mu_j] = \nu[\ln\mu_i] + \nu[\ln\mu_j] - 2\nu[\ln\mu_i, \ln\mu_j]; \quad (24)$$

the result

$$\nu[\ln\mu_i, \ln\mu_j] = \ln(\mu_i - \mu_j), \quad (25)$$

which also follows from the inverse scattering method; and the identity

$$(r^2 + \mu_i\mu_j)(\mu_i - \mu_j) = 2(\alpha_i - \alpha_j)\mu_i\mu_j, \quad (26)$$

one obtains following expressions for the metric function ν

$$\nu_{BH} = \ln\left[\frac{(r^2 + \mu_1\mu_2)^2}{(r^2 + \mu_1^2)(r^2 + \mu_2^2)}\right], \quad (27)$$

$$\nu_R = 4\lambda^2 \ln\left[\frac{(r^2 + \mu_3\mu_4)^2}{(r^2 + \mu_3^2)(r^2 + \mu_4^2)}\right]. \quad (28)$$

V. SUPERPOSITION OF DISK, BLACK HOLE AND RODS

We now consider the superposition illustrated in Fig. 1: a black hole with mass M whose center is on $z = 0$, two rods with equal mass density λ, each one with mass $\mathcal{M}$ located along $[-c_2, -c_1]$ and $[c_1, c_2]$ on the z axis, and a disk on the plane $z = 0$ constructed with the "displace, cut and reflect method" from the Chazy-Curzon solution with mass m, whose singularity lies on $z = -a$:

$$\phi_D = -\frac{2m}{\sqrt{r^2 + (|z| + a)^2}}. \quad (29)$$

It should be remembered that in Weyl coordinates a black hole with mass M is represented by a rod with length $2M$; thus in Fig. 1 we put a dotted circle around the rod in the middle. Such a configuration is not gravitationally stable; a consequence of the nonlinearity of Eq. (2b) is the appearance of gravitationally inert singular structures like struts between the rods and the black hole that keeps them apart. Also in the superposition of the disk with the black hole, superlumial regions ($V^2 > 1$) exist because there is matter up to the event horizon.

The metric function ϕ of the superposition can be expressed as

$$\phi = -2\lambda \ln\left(\frac{\mu_3}{\mu_4}\right) + \ln\left(\frac{\mu_1}{\mu_2}\right) - 2\lambda \ln\left(\frac{\mu_5}{\mu_6}\right) + \phi_D, \quad (30)$$

with $\mu_5 = -c_1 - z + \sqrt{r^2 + (c_1 + z)^2}$ and $\mu_6 = -c_2 - z + \sqrt{r^2 + (c_2 + z)^2}$.

Now we consider the case when both rods just touch the horizon of the black hole, that is, when $c_1 = M$. Then

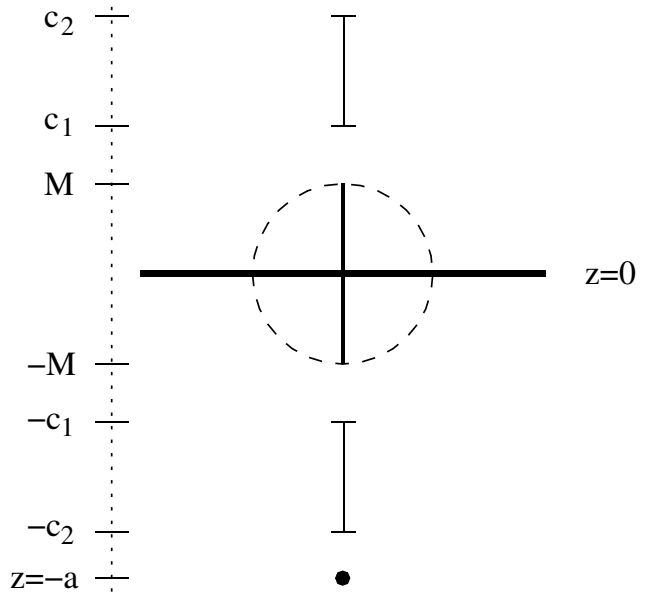

FIG. 1. Superposition of a black hole with mass M, two rods, and a Chazy-Curzon disk on the plane $z = 0$.

$\mu_4 = \mu_2$ and $\mu_5 = \mu_1$. From Eqs. (13), (14), and (8), we get following conditions:

$$\sigma > 0 \rightarrow \sqrt{\tilde{r}^2 + \tilde{c}_2^2}\Big[(\tilde{r}^2 + \tilde{a}^2)^{3/2}\Big(\sqrt{1+\tilde{r}^2} - 1\Big) - \alpha\tilde{r}^2\sqrt{1+\tilde{r}^2}\Big] + 2\lambda(\tilde{r}^2 + \tilde{a}^2)^{3/2} \times\Big(\sqrt{\tilde{r}^2 + \tilde{c}_2^2} - \tilde{c}_2\sqrt{1+\tilde{r}^2}\Big) > 0, \quad (31)$$

$$p > 0 \rightarrow \sqrt{\tilde{r}^2 + \tilde{c}_2^2}\Big[\alpha\tilde{r}^2\sqrt{1+\tilde{r}^2} + (\tilde{r}^2 + \tilde{a}^2)^{3/2}\Big] - 2\lambda(\tilde{r}^2 + \tilde{a}^2)^{3/2}\Big(\sqrt{\tilde{r}^2 + \tilde{c}_2^2} - \tilde{c}_2\sqrt{1+\tilde{r}^2}\Big) > 0, \quad (32)$$

$$V^2 < 1 \rightarrow \sqrt{\tilde{r}^2 + \tilde{c}_2^2}\Big[2\alpha\tilde{r}^2\sqrt{1+\tilde{r}^2} + (\tilde{r}^2 + \tilde{a}^2)^{3/2} \times\Big(2 - \sqrt{1+\tilde{r}^2}\Big)\Big] - 4\lambda(\tilde{r}^2 + \tilde{a}^2)^{3/2} \times\Big(\sqrt{\tilde{r}^2 + \tilde{c}_2^2} - \tilde{c}_2\sqrt{1+\tilde{r}^2}\Big) < 0, \quad (33)$$

where $\tilde{r} = r/M$, $\tilde{a} = a/M$, $\tilde{c}_2 = c_2/M$, $\alpha = m/M$, $\beta = \mathcal{M}/M$ and $\lambda = \mathcal{M}/(c_2 - M) = \beta/(\tilde{c}_2 - 1)$. The conditions imposed are that of weak energy ($\sigma > 0$), azimuthal pressure ($p > 0$) and sublumial velocity ($V^2 < 1$) of counter-rotation of particles on the disk. For $\tilde{r} \rightarrow \infty$, all three conditions are satisfied. In the regions where $V^2 < 1$, the weak energy condition is always satisfied, as can be seen by inequalities (31) and (33).

Figure 2(a)–2(c)shows curves of $V^2 = 1$ (dotted curves) and of $hdh/dr = 0$ (solid curves) as function

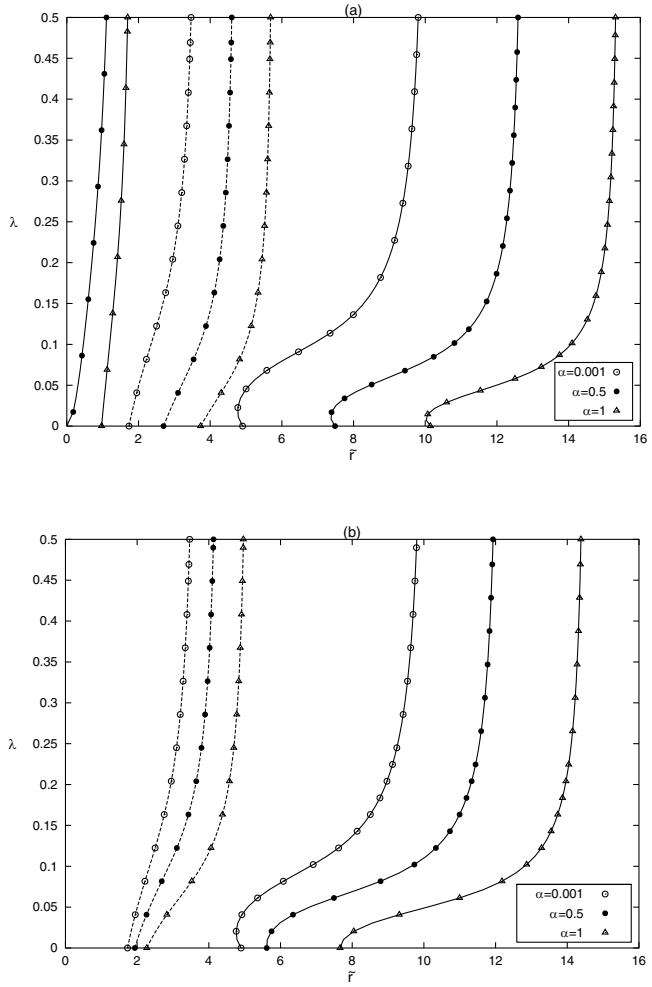

FIG. 2. Curves of $V^2 = 1$ (dotted curves) and of $hdh/dr = 0$ (solid curves) for the Chazy-Curzon disk in presence of a black hole and two rods. We keep the mass of each rod constant $\beta = 0.5$ and vary its mass density λ. In (a)-(b) we take, respectively, $\tilde{a} = 1$ and $\tilde{a} = 3$.

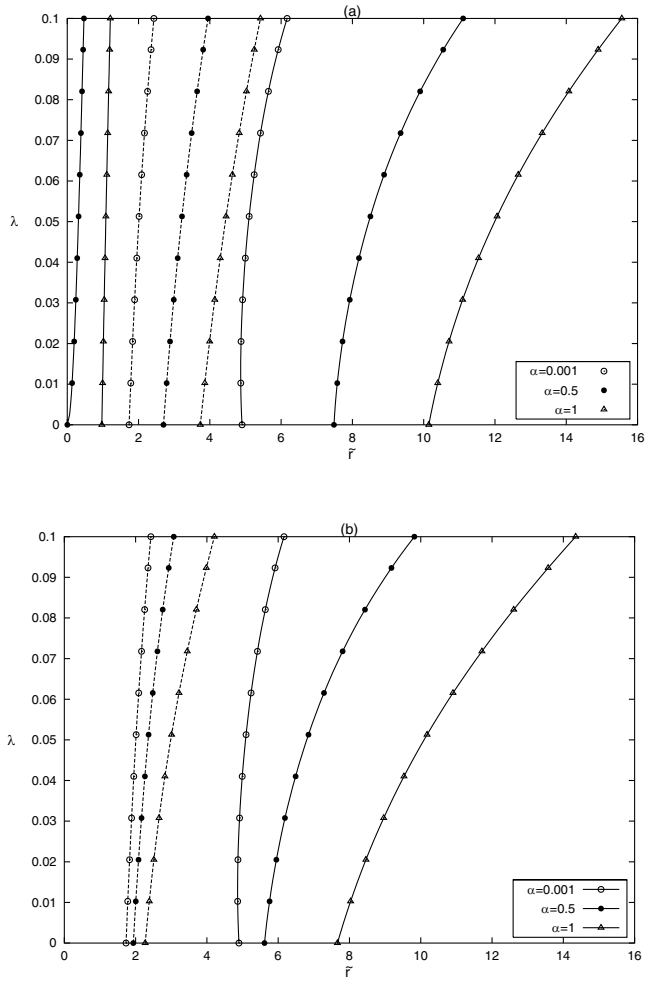

FIG. 3. Curves of $V^2 = 1$ (dotted curves) and of $hdh/dr = 0$ (solid curves) for the Chazy-Curzon disk in presence of a black hole and two rods. We keep the length of each rod constant $\tilde{c}_2 = 11$ and vary its mass density λ (or equivalent, its mass). In (a)-(b) we take, respectively, $\tilde{a} = 1$ and $\tilde{a} = 3$.

of λ and $\tilde{r}$ for three different values of α. The mass of each rod is kept constant $\beta = 0.5$ and the cut parameter takes values $\tilde{a} = 1$ and $\tilde{a} = 3$ in 2(a) and 2(b), respectively. At the right of each dotted curve we have $V^2 < 1$ and the unstable regions of the disk appear between the curves of $hdh/dr = 0$. We note that in general with increasing mass of the disk and smaller length of the rods, the disk becomes more unstable and the regions of superlumial velocity also increase. There is, however, an interval of values for the rod's mass density where the zone of stability is increased, as can be seen in the lower part of the curve $hdh/dr = 0$ for $\alpha = 0.001$ in Fig. 2(a). This is probably due to the prolate quadrupole moment of the rods, which scale as $\mathcal{M}l^2$, where l is their length. Thus, for larger rods, the effect of prolate deformations may overwhelm the effect of the oblate quadrupole moment of the disk, and increase stability (see [39] for a detailed discussion of the effect of quadrupolar fields on the stability of circular orbits).

Figure 3(a) and 3(b)shows again curves of $V^2 = 1$ (dotted curves) and of $hdh/dr = 0$ (solid curves) as function of λ and $\tilde{r}$ for three different values of α, but now the length of each rod is kept constant ($\tilde{c}_2 = 11$) and the cut parameter takes values $\tilde{a} = 1$ and $\tilde{a} = 3$ in 3(a) and 3(b), respectively. With increasing masses of the disk and of the rods, the zones of instability and superlumial velocity of the disk are enhanced. In Fig. 4(a)–4(d) we plot the energy density $\bar{\sigma} = M\sigma$, azimuthal pressure $\bar{p} = Mp$, square of the counter-rotating velocity V and specific angular momentum $\bar{h} = Mh$ as functions of $\tilde{r}$ for $\tilde{a} = 3$, $\alpha = 1$, $\tilde{c}_2 = 11$ (constant length) and different values of the rod's linear mass density λ. The curves were computed using Eqs. (13)–(17), (8), (9), and (30). The expression for the corresponding metric function ν is given in the Appendix. Energy density is lowered for a fixed radius as the rods become more massive, while pressure is slightly increased. Velocity of counter-rotation and specific angular momentum are enhanced by increasing mass of the rods, as can also be deduced from Fig. 3(b).

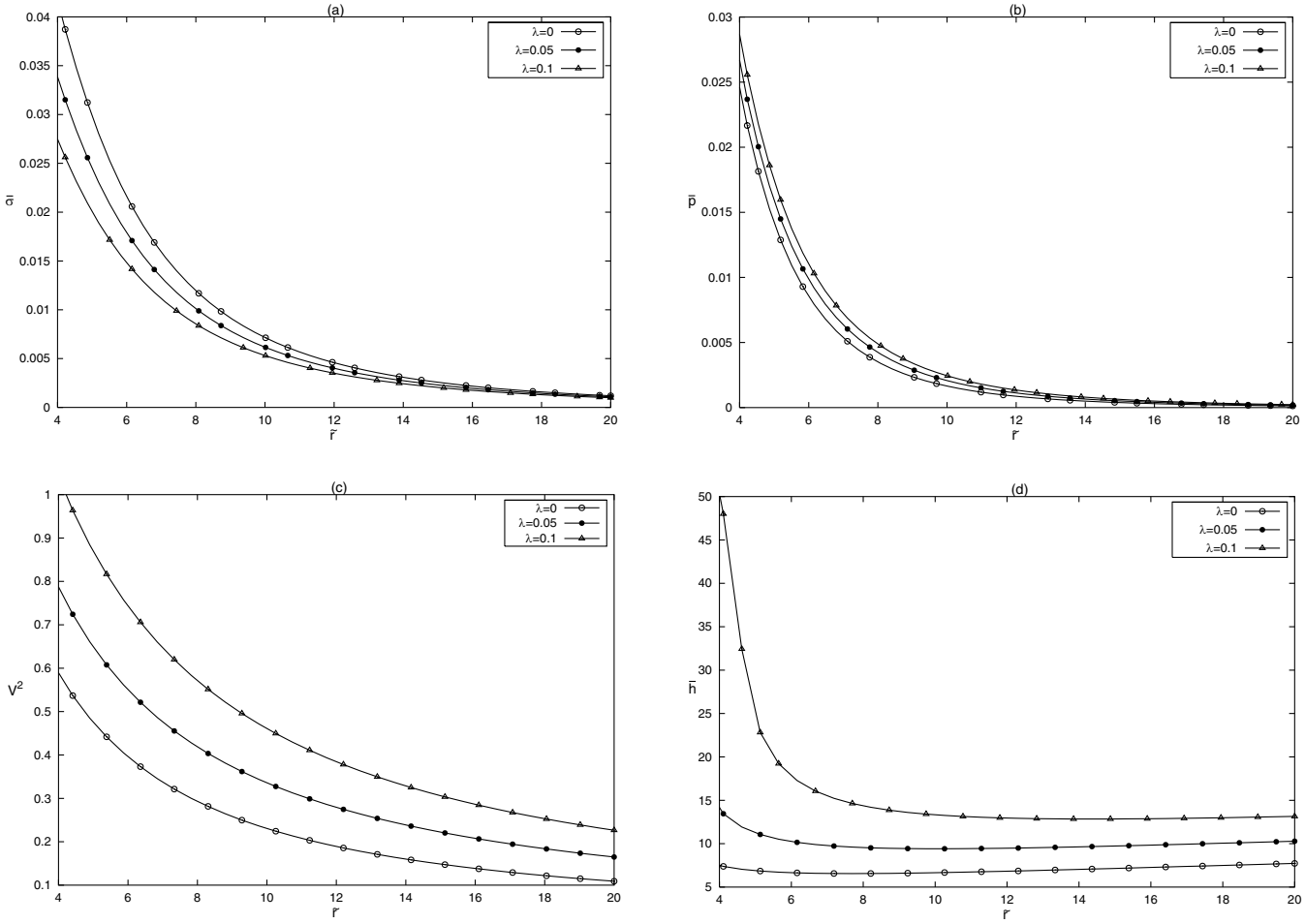

FIG. 4. (a) Energy density $\bar{\sigma}$, (b) azimuthal pressure $\bar{p}$, (c) counter-rotating velocity V^2 and (d) specific angular momentum $\bar{h}$ as functions of $\tilde{r}$ for $\alpha = 1$, $\tilde{a} = 3$, $\tilde{c}_2 = 11$ and three different values for the rod's mass density λ.

VI. HORIZONTAL AND VERTICAL OSCILLATIONS OF THE DISK

It is interesting to study the disk stability through the computation of horizontal (epicyclic) and vertical oscillation frequencies from perturbations of equatorial circular geodesics. Semerák and Žáček [40] have done such calculations for the superposition of a Schwarzschild black hole with the Lemos-Letelier disk. They found that heavier disks are more stable with respect to horizontal perturbations near their inner rims, whereas they are less stable with respect to vertical perturbations. For astrophysical relevance, it is important to determine not only the stability of circular motion on the disk plane, but also stability in the vertical direction.

Using the perturbed equations for equatorial circular geodesics, the epicyclic frequency with respect to infinity ω_h and the vertical oscillation frequency with respect to infinity ω_v for the metric (1) are given by (see [40] for a detailed deduction)

$$\omega_h^2 = \frac{e^{2\phi-\nu}}{2-r\phi_{,r}}\left(\phi_{,rr} + r\phi_{,r}^3 - 3\phi_{,r}^2 + \frac{3}{r}\phi_{,r}\right), \tag{34}$$

$$\omega_v^2 = \frac{e^{2\phi-\nu}}{2-r\phi_{,r}}[\phi_{,zz} - 2\phi_z^2(1-r\phi_{,r})]. \tag{35}$$

In Eq. (35) the function ϕ_z is obtained from the limit $\lim_{z\to 0^{\pm}}\phi_z$ and $\phi_{,zz}$ follows from Eq. (2a). Stable horizontal and vertical orbits are only possible where $\omega_h^2 > 0$ and $\omega_v^2 > 0$, respectively. Note that condition $\omega_h^2 > 0$ is equivalent to condition (10) which follows from Rayleigh stability criteria.

We compute first the frequencies for an isolated Chazy-Curzon disk, since is seems that such a calculation has not been done before for this class of disks. In Fig. 5(a) we plot the epicyclic frequency as functions of radius r/m and cut parameter a/m. For $a/m > 1.015$ the disks always are stable and the epicyclic frequency is lowered for

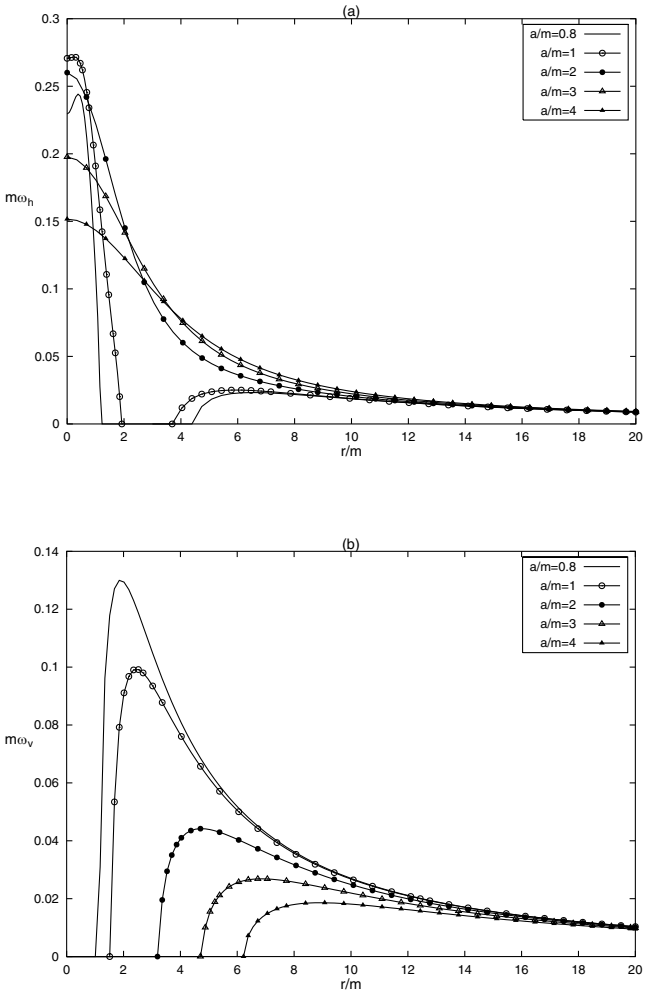

FIG. 5. Radial profiles of (a) the epicyclic frequency $m\omega_h$ and (b) the vertical oscillation frequency $m\omega_v$ for an isolated Chazy-Curzon disk.

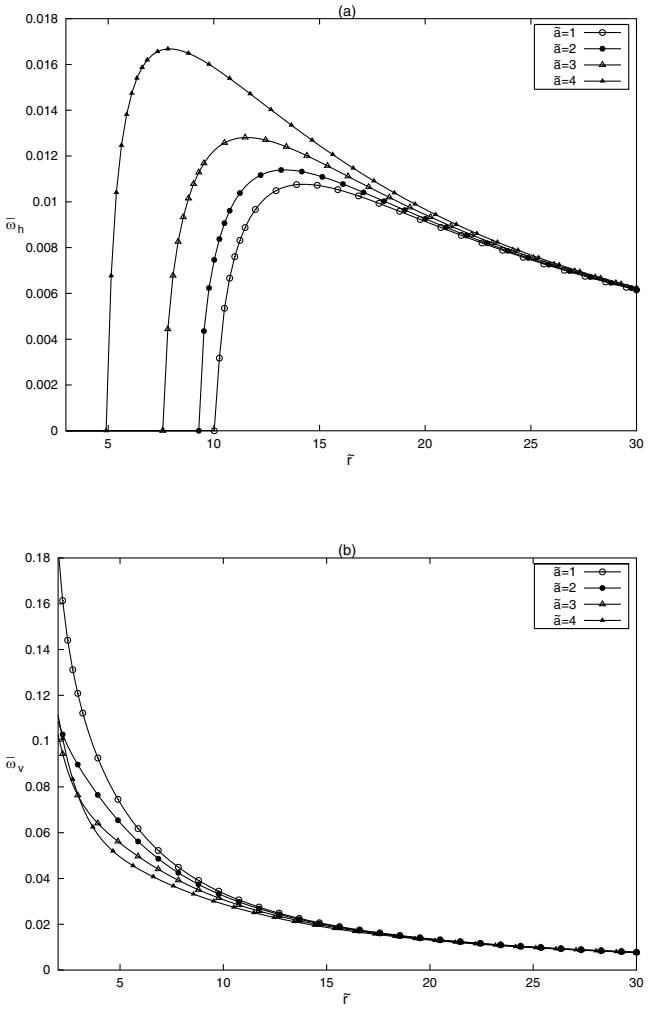

FIG. 6. Radial profiles of (a) horizontal and (b) vertical oscillation frequencies of Chazy-Curzon disk with a black hole without rods. Parameters: $\alpha = 1$, $\tilde{a} = 1, 2, 3$ and 4.

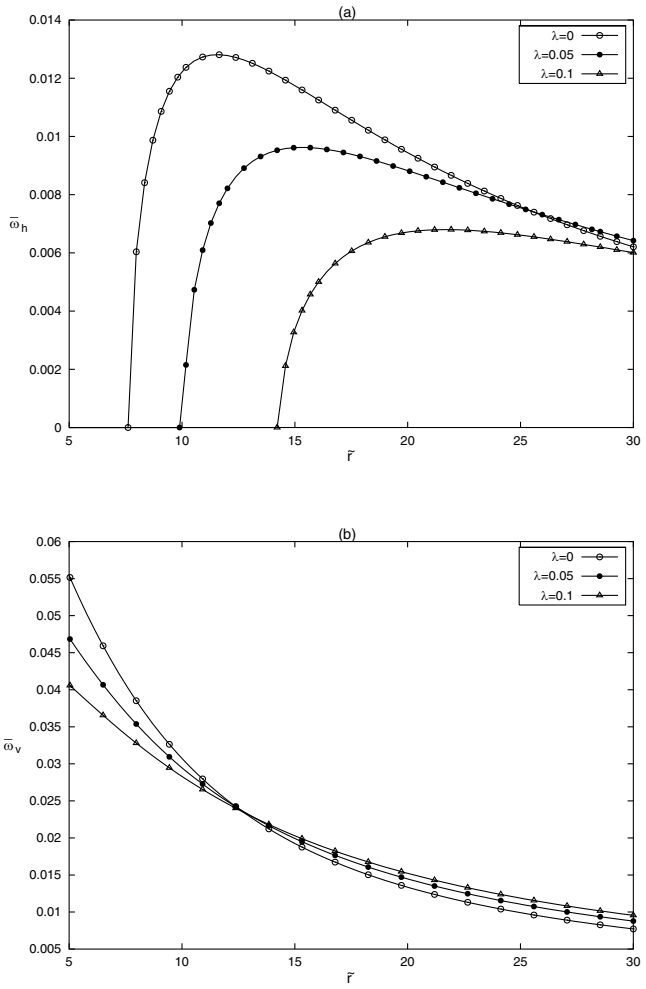

FIG. 7. Radial profiles of (a) horizontal and (b) vertical oscillation frequencies of Chazy-Curzon disk with black hole and rods. Parameters are $\tilde{c}_2 = 11$, $\alpha = 1$, $\tilde{a} = 3$, $\lambda = 0, 0.05$ and 0.1.

less relativistic disks. Highly relativistic disks (curve with $a/m = 0.8$ for example) develop annular regions of instability. The curves of vertical oscillation frequencies are depicted in Fig. 5(b). We note that in this case highly relativistic disks are more stable in the vertical direction. In Eq. (35) the term with ϕ_z is small compared to $\phi_{,zz}$, thus if we consider only

$$\phi_{,zz} = \frac{2m}{(r^2 + a^2)^{5/2}}(r^2 - 2a^2), \tag{36}$$

we note that vertical oscillations are zero at $r = a\sqrt{2}$, so the regions of vertical stability are enlarged as the cut parameter a is decreased.

Now we consider the superposition of a Curzon disk and a black hole *without* rods. Figure 6 shows curves of (a) horizontal $\bar{\omega}_h = M\omega_h$ and (b) vertical $\bar{\omega}_v = M\omega_v$ oscillation frequencies of the disk with $\alpha = 1$ and four different values of the "cut" parameter $\tilde{a}$. Now we always have regions of horizontal instability that begin at the innermost stable circular orbit and decrease for less relativistic disks. With respect to vertical oscillations, it is seen from Fig. 6(b) that there are no regions of vertical instabilities. Thus one can conclude that the black hole destabilizes the Curzon disk in the horizontal direction, whereas the opposite is true for the vertical direction.

In Fig. 7(a) and 7(b) we graph again $\bar{\omega}_h = M\omega_h$ and $\bar{\omega}_v = M\omega_v$, respectively, for the Chazy-Curzon disk with black hole and rods, with their length fixed and vary the linear mass density λ. As expected from the curves of Fig. 3(b), the more massive the rods, the larger are the disk's unstable regions in the horizontal direction. The rods also tend to lower the vertical oscillation frequencies near the disk's center, but unstable regions do not appear.

VII. GEODESIC ORBITS

In the previous section perturbations of equatorial circular geodesics were used to discuss disk stability for

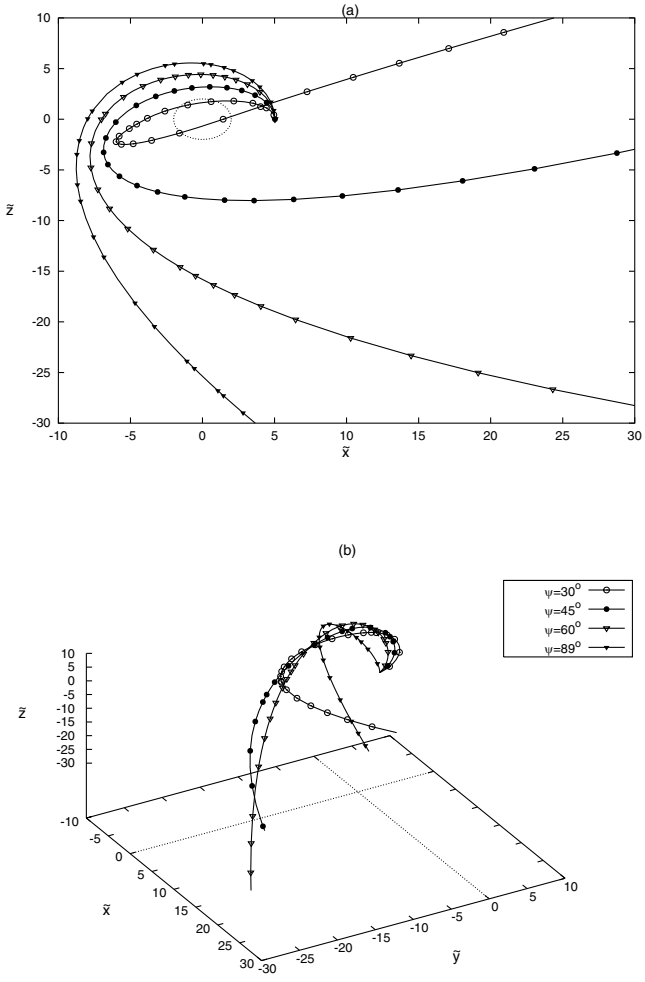

FIG. 8. Geodesic orbits for the superposition Curzon disk + black hole without rods. Parameters: $\alpha = 1$, $\tilde{a} = 3$, $\mathcal{E} \approx 1.01$, $\tilde{r}_0 = 3.9$. (a) Projection on the $x - z$ plane of the curves in (b).

the system disk + blackhole + rods. Now we solve numerically the geodesic equations of motion

$$\ddot{x}^{\mu} + \Gamma^{\mu}_{\alpha\beta}\dot{x}^{\alpha}\dot{x}^{\beta} = 0, \tag{37}$$

for metric Eq. (1), where $\Gamma^{\mu}_{\alpha\beta}$ are the Christoffel symbols and the dot denote differentiation with respect to the proper time. Defining the orthonormal tetrad $\{V^a, W^a, Y^a, Z^a\}$ where

$$V^a = e^{-\phi/2}(1, 0, 0, 0), \tag{38a}$$

$$W^a = e^{(\phi-\nu)/2}(0, 1, 0, 0), \tag{38b}$$

$$Y^a = e^{(\phi-\nu)/2}(0, 0, 1, 0), \tag{38c}$$

$$Z^a = \frac{e^{\phi/2}}{r}(0, 0, 0, 1), \tag{38d}$$

the tetrad components of the four-velocity v^a read

$$v^a = \gamma(1, v\sin\psi\cos\chi, v\sin\psi\sin\chi, v\cos\psi), \tag{39}$$

with $\gamma = 1/\sqrt{1-v^2}$. The specific energy and angular momentum of the test particle are

$$\mathcal{E} = e^{\phi}\dot{t} = e^{\phi/2}\gamma, \tag{40}$$

$$h = r^2 e^{-\phi}\dot{\varphi} = re^{-\phi/2}\gamma v\cos\psi. \tag{41}$$

As initial conditions we take a position at radius r_0 on the disk's plane and components of the four-velocity $v_0^a = \gamma(1, 0, v_0\sin\psi, v_0\cos\psi)$, where v_0 is equal to the tangential velocity of circular orbits at radius r_0. We choose initial radii such that the energy is slightly higher than the escape energy. Figure 8(a) and 8(b)shows the orbits of particles in the presence of the black hole and Curzon disk without rods. The parameters are $\alpha = 1$, $\tilde{a} = 3$, $\tilde{r}_0 = 3.9$, $\mathcal{E} \approx 1.01$ and different initial angles ψ. Figure 8(a) is a projection of the orbits on the $x - z$ plane. The coordinates have been transformed from Weyl to Schwarzschild coordinates $(t, \mathsf{r}, \theta, \varphi)$ via the relations

$$r = \sqrt{\mathsf{r}(\mathsf{r} - 2M)}\sin\theta, \qquad z = (\mathsf{r} - M)\cos\theta, \tag{42}$$

and then to $x = \mathsf{r}\sin\theta\cos\varphi$, $y = \mathsf{r}\sin\theta\sin\varphi$ and $z = \mathsf{r}\cos\theta$.

In Fig. 9(a)–9(d) we have computed some orbits now with the rods. The parameters are $\alpha = 1$, $\tilde{a} = 3$,

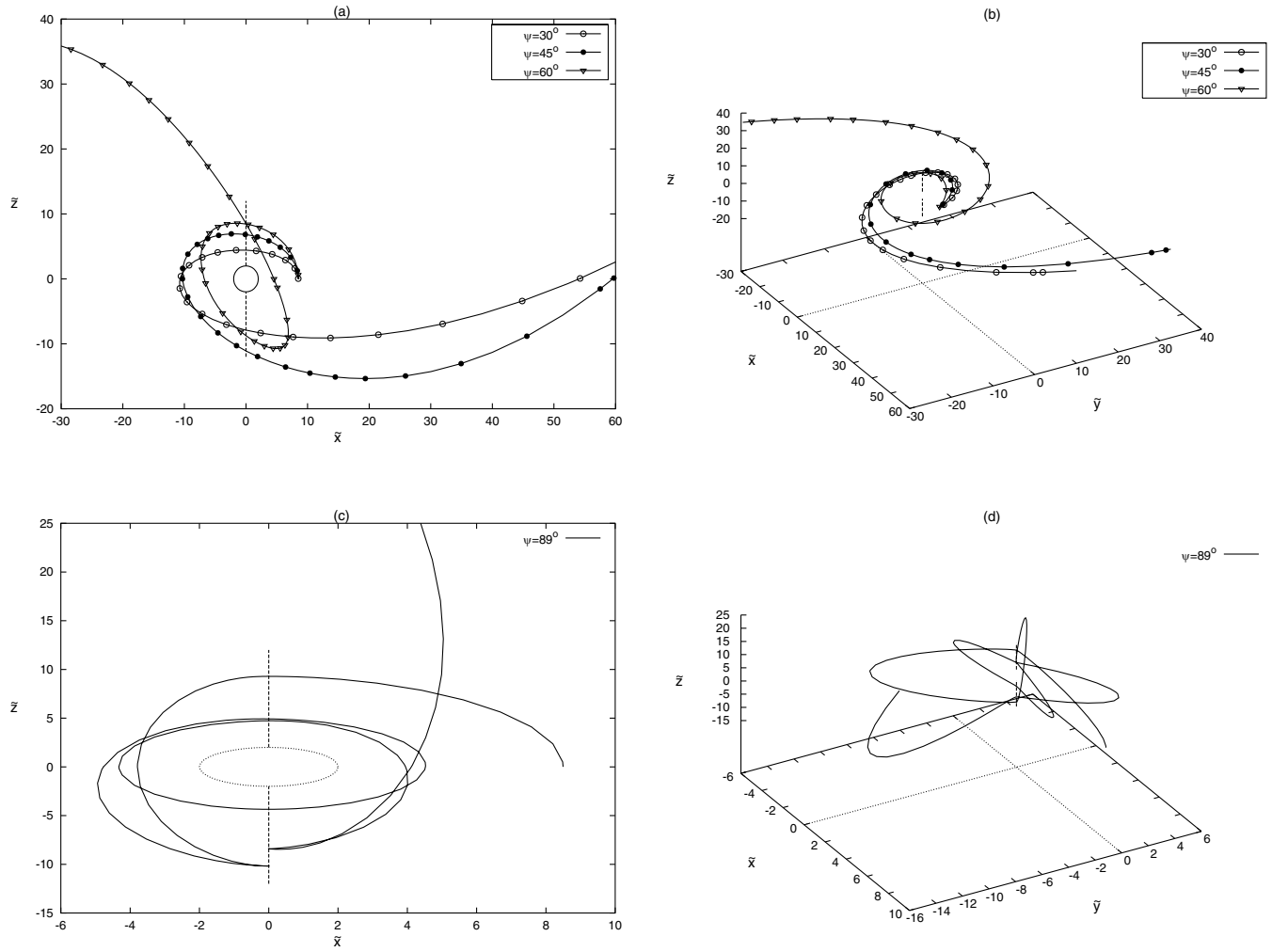

FIG. 9. Geodesic orbits for the superposition Curzon disk + black hole with rods. Parameters: $\alpha = 1$, $\tilde{a} = 3$, $\lambda = 0.1$, $\tilde{c}_2 = 11$, $\mathcal{E} \approx 1.01$ $\tilde{r}_0 = 7.43$. The curve for $\psi = 89^o$ is displayed in (c) and (d) for better visualization.

$\tilde{r}_0 = 7.43$, $\lambda = 0.1$, $\tilde{c}_2 = 11$, $\mathcal{E} \approx 1.01$ and different initial angles ψ. The orbit with $\psi = 89^o$ has been placed in a separate graph for better visualization. For low initial angles, the rods have little effect on the trajectories, but this is not true as the particles approach the z axis. The orbit in Fig. 9(c) and 9(d) even suggests that we can expect chaotic behavior for orbits that pass very near the rods. In fact, it has been shown [41] that prolate quadrupole deformations can introduce chaotic motion of geodesic test particles. In the oblate case, only regular motion was found.

VIII. DISCUSSION

We presented a very simplified, although exact, general relativistic model of an active galactic nuclei based on a superposition of a Schwarzschild black hole, a Chazy-Curzon disk and two rods placed on the symmetry axis, representing jets. We found that the presence of the rods enhances the disk regions with superlumial velocities. Using an extension of Rayleigh criteria of stability, it was found that in general the rods also increase the regions of instability, but when the rods are large and the disk's mass is low they can contribute to stabilize the disk. Also disk stability in the vertical direction was studied through perturbation of circular geodesics. The rods contribute to lower the vertical oscillation frequencies near the disk's center. Some geodesic orbits calculated numerically for the system blackhole + disk + rods show the possibility of chaotic trajectories near the rods.

The model here presented should be viewed as a first approach. As was stated in the introduction, more realistic models of active galactic nuclei should incorporate rotation and electromagnetic fields. However, the analysis of such a model would not be trivial, because of the large number of free parameters involved.

APPENDIX

The metric function Eq. (2b) for the superposition of a black hole, two rods and a disk generated from Chazy-Curzon solution can be calculated as follows. We rewrite potential Eq. (30) as

$$\phi = \phi_{R1} + \phi_{BH} + \phi_{R2} + \phi_D^+, \tag{A1}$$

where

$$\phi_{R1} = -2\lambda \ln\left(\frac{\mu_3}{\mu_4}\right), \qquad \phi_{BH} = -2\lambda \ln\left(\frac{\mu_1}{\mu_2}\right),$$
$$\phi_{R2} = -2\lambda \ln\left(\frac{\mu_5}{\mu_6}\right), \qquad \phi_D^+ = \frac{m}{\epsilon} \ln\left(\frac{\mu_7}{\mu_8}\right), \tag{A2}$$

with $\mu_7 = -a - \epsilon - z + \sqrt{r^2 + (-a - \epsilon - z)^2}$ and $\mu_8 = -a + \epsilon - z + \sqrt{r^2 + (-a + \epsilon - z)^2}$. In the limit $\epsilon \to 0$ expression for ϕ_D^+ reduces to the Chazy-Curzon disk Eq. (29) on $z > 0$. Thus all terms can be expressed as μ potentials. Using repeatedly properties (24)–(26) we get

$$\begin{aligned}\nu[\phi_{R1} + \phi_{BH} + \phi_{R2} + \phi_D^+] &= \nu[\phi_{R1}] + \nu[\phi_{BH}] + \nu[\phi_{R2}] + \nu[\phi_D^+] \\ &\quad + 2\nu[\phi_{R1}, \phi_{BH}] + 2\nu[\phi_{R1}, \phi_{R2}] + 2\nu[\phi_{R1}, \phi_D^+] \\ &\quad + 2\nu[\phi_{BH}, \phi_{R2}] + 2\nu[\phi_{BH}, \phi_D^+] + 2\nu[\phi_{R2}, \phi_D^+],\end{aligned} \tag{A3}$$

with

$$\nu[\phi_{R1}] = 4\lambda^2 \ln\left[\frac{(r^2 + \mu_3\mu_4)^2}{(r^2 + \mu_3^2)(r^2 + \mu_4^2)}\right], \qquad \nu[\phi_{BH}] = \ln\left[\frac{(r^2 + \mu_1\mu_2)^2}{(r^2 + \mu_1^2)(r^2 + \mu_2^2)}\right],$$
$$\nu[\phi_{R2}] = 4\lambda^2 \ln\left[\frac{(r^2 + \mu_5\mu_6)^2}{(r^2 + \mu_5^2)(r^2 + \mu_6^2)}\right], \qquad \nu[\phi_D^+] = -\frac{m^2 r^2}{[r^2 + (z + a)^2]^2},$$
$$\nu[\phi_{R1}, \phi_{BH}] = 2\lambda \ln\left[\frac{(r^2 + \mu_1\mu_3)(r^2 + \mu_2\mu_4)}{(r^2 + \mu_1\mu_4)(r^2 + \mu_2\mu_3)}\right], \qquad \nu[\phi_{R1}, \phi_{R2}] = 4\lambda^2 \ln\left[\frac{(r^2 + \mu_3\mu_6)(r^2 + \mu_4\mu_5)}{(r^2 + \mu_3\mu_5)(r^2 + \mu_4\mu_6)}\right],$$
$$\nu[\phi_{R1}, \phi_D^+] = \frac{2\lambda m}{(a + c_1)(a + c_2)\sqrt{r^2 + (a + z)^2}}\Big[(a + c_2)\sqrt{r^2 + (c_1 - z)^2} - (a + c_1)\sqrt{r^2 + (c_2 - z)^2} + (c_1 - c_2)\sqrt{r^2 + (a + z)^2}\Big],$$
$$\nu[\phi_{BH}, \phi_{R2}] = 2\lambda \ln\left[\frac{(r^2 + \mu_1\mu_5)(r^2 + \mu_2\mu_6)}{(r^2 + \mu_1\mu_6)(r^2 + \mu_2\mu_5)}\right],$$
$$\nu[\phi_{BH}, \phi_D^+] = \frac{m}{(a^2 - M^2)\sqrt{r^2 + (a + z)^2}}\Big[(a + M)\sqrt{r^2 + (M + z)^2} - (a - M)\sqrt{r^2 + (M - z)^2} - 2M\sqrt{r^2 + (a + z)^2}\Big],$$
$$\nu[\phi_{R2}, \phi_D^+] = \frac{2\lambda m}{(a - c_1)(a - c_2)\sqrt{r^2 + (a + z)^2}}\Big[(c_2 - a)\sqrt{r^2 + (c_1 + z)^2} - (c_1 - a)\sqrt{r^2 + (c_2 + z)^2} + (c_1 - c_2)\sqrt{r^2 + (a + z)^2}\Big]. \tag{A4}$$

In the particular case $c_1 = M$ ($\mu_4 = \mu_2$ and $\mu_5 = \mu_1$), and on $z = 0$, Eq. (A2) simplifies to

$$\nu[\phi_{R1}+\phi_{BH}+\phi_{R2}+\phi_D^+] = \ln\left[\frac{r^{16\lambda^2-8\lambda+2}(r^2+\mu_1\mu_6)^{8\lambda^2-4\lambda}(r^2+\mu_2\mu_3)^{8\lambda^2-4\lambda}}{(r^2+c_2^2)^{4\lambda^2}(r^2+M^2)^{4\lambda^2-4\lambda+1}(r^2+\mu_1\mu_3)^{8\lambda^2-4\lambda}(r^2+\mu_2\mu_6)^{8\lambda^2-4\lambda}}\right] - \frac{m^2r^2}{(r^2+a^2)^2}$$
$$+\frac{8\lambda m}{(a^2-c_2^2)(a^2-M^2)\sqrt{r^2+a^2}}\Big[c_2(a^2-M^2)\sqrt{r^2+c_2^2} - M(a^2-c_2^2)\sqrt{r^2+M^2}$$
$$+(M-c_2)(a^2+Mc_2)\sqrt{r^2+a^2}\Big] + 4mM\frac{(\sqrt{r^2+M^2}-\sqrt{r^2+a^2})}{(a^2-M^2)\sqrt{r^2+a^2}}. \quad \text{(A5)}$$

ACKNOWLEDGMENTS

D.V. thanks CAPES for financial support. P. S. L. thanks CNPq and FAPESP for financial support.

[1] *Jets from Stars and Galactic Nuclei*, edited by W. Kundt (Springer, New York, 1996.
[2] J. H. Krolik, *Active Galactic Nuclei: from the Central Black Hole to the Galactic Environment* (Princeton University Press, Princeton, New Jersey, 1999.
[3] R. D. Blandford, Prog. Theor. Phys. Suppl. **143**, 182 (2001).
[4] W. A. Bonnor and A. Sackfield, Commun. Math. Phys. **8**, 338 (1968).
[5] T. Morgan and L. Morgan, Phys. Rev. **183**, 1097 (1969).
[6] L. Morgan and T. Morgan, Phys. Rev. D **2**, 2756 (1970).
[7] D. Lynden-Bell and S. Pineault, Mon. Not. R. Astron. Soc. **185**, 679 (1978).
[8] P. S. Letelier and S. R. Oliveira, J. Math. Phys. **28**, 165 (1987).
[9] J. P. S. Lemos, Classical Quantum Gravity **6**, 1219 (1989).
[10] J. P. S. Lemos and P. S. Letelier, Classical Quantum Gravity **10**, L75 (1993).
[11] J. Bičák, D. Lynden-Bell, and J. Katz, Phys. Rev. D **47**, 4334 (1993).
[12] J. Bičák, D. Lynden-Bell, and C. Pichon, Mon. Not. R. Astron. Soc. **265**, 126 (1993).
[13] J. P. S. Lemos and P. S. Letelier, Phys. Rev. D **49**, 5135 (1994).
[14] J. P. S. Lemos and P. S. Letelier, Int. J. Mod. Phys. D **5**, 53 (1996).
[15] G. González and O. A. Espitia, Phys. Rev. D **68**, 104028 (2003).
[16] G. García and G. González, Phys. Rev. D **69**, 124002 (2004).
[17] J. Bičák and T. Ledvinka, Phys. Rev. Lett. **71**, 1669 (1993).
[18] G. González and P. S. Letelier, Phys. Rev. D **62**, 064025 (2000).
[19] D. Vogt and P. S. Letelier, Phys. Rev. D **68**, 084010 (2003).
[20] D. Vogt and P. S. Letelier, "Exact Relativistic Static Charged Perfect Fluid Disks" (to be published).
[21] G. González and P. S. Letelier, Phys. Rev. D **69**, 044013 (2004).
[22] C. Klein, Classical Quantum Gravity **14**, 2267 (1997).
[23] G. Neugebauer and R. Meinel, Phys. Rev. Lett. **75**, 3046 (1995).
[24] C. Klein and O. Richter, Phys. Rev. Lett. **83**, 2884 (1999).
[25] C. Klein, Phys. Rev. D **63**, 064033 (2001).
[26] J. Frauendiener and C. Klein, Phys. Rev. D **63**, 084025 (2001).
[27] C. Klein, Phys. Rev. D **65**, 084029 (2002).
[28] C. Klein, Phys. Rev. D **68**, 027501 (2003).
[29] C. Klein, Ann. Phys. **12**, 599 (2003).
[30] T. Zellerin and O. Semerák, Classical Quantum Gravity **17**, 5103 (2000).
[31] V. Karas, J. M. Huré, and O. Semerák, Classical Quantum Gravity **21**, R1 (2004).
[32] H. Weyl, Ann. Phys. **54**, 117 (1917).
[33] H. Weyl, Ann. Phys. **59**, 185 (1919).
[34] G. G. Kuzmin, Astron. Zh. **33**, 27 (1956).
[35] J. P. S. Lemos, Mon. Not. R. Astron. Soc. **230**, 451 (1988).
[36] Lord Rayleigh, Proc. R. Soc. London A **93**, 148 (1917); see also L. D. Landau and E. M. Lifshitz, *Fluid Mechanics* (Pergamon Press, Oxford, 1987), 2nd ed., p. 27.
[37] V. A. Belinsky and V. E. Zakharov, Zh. Eksp. Teor. Fiz. **75**, 1955 (1978) [Sov. Phys. JETP **48**, 985 (1978)].
[38] V. A. Belinsky and V. E. Zakharov, Zh. Eksp. Teor. Fiz. **77**, 3 (1979) [Sov. Phys. JETP **50**, 1 (1979)].
[39] P. S. Letelier, Phys. Rev. D **68**, 104002 (2003).
[40] O. Semerák and M. Žáček, Publ. Astron. Soc. Jpn. **52**, 1067 (2000).
[41] E. Gueron and P. S. Letelier, Phys. Rev. E **63**, 035201(R) (2001); **66**, 046611 (2002).